

CIMIL-CRC: a clinically-informed multiple instance learning framework for patient-level colorectal cancer molecular subtypes classification from H&E stained images

Hadar Hezi^a, Matan Gelber^b, Alexander Balabanov^b, Yosef E. Maruvka^c, Moti Freiman^{a,*}

^a*Faculty of Biomedical Engineering, Technion – Israel Institute of Technology, Technion City, Haifa 3200003, Israel*

^b*Faculty of Electrical and Computer Engineering, Technion – Israel Institute of Technology, Technion City, Haifa 3200003, Israel*

^c*Faculty of Food Engineering and Biotechnology, Technion – Israel Institute of Technology, Technion City, Haifa 3200003, Israel*

Abstract

Treatment approaches for colorectal cancer (CRC) are highly dependent on the molecular subtype, as immunotherapy has shown efficacy in cases with microsatellite instability (MSI) but is ineffective for the microsatellite stable (MSS) subtype. There is promising potential in utilizing deep neural networks (DNNs) to automate the differentiation of CRC subtypes by analyzing Hematoxylin and Eosin (H&E) stained whole-slide images (WSIs). Due to the extensive size of WSIs, Multiple Instance Learning (MIL) techniques are typically explored. However, existing MIL methods focus on identifying the most representative image patches for classification, which may result in the loss of critical information. Additionally, these methods often overlook clinically relevant information, like the tendency for MSI class tumors to predominantly occur on the proximal (right side) colon. We introduce ‘CIMIL-CRC’, a DNN framework that: 1) solves the MSI/MSS MIL problem by efficiently combining a pre-trained feature extraction model with principal component analysis (PCA) to aggregate information from all patches, and 2) integrates clinical priors, particularly the tumor location within the colon, into the model to enhance patient-level classification accuracy. We assessed our CIMIL-CRC method using the average area under the curve (AUC) from a 5-fold cross-validation experimental setup for model development on the TCGA-CRC-DX cohort, contrasting it with a baseline patch-level classification, MIL-only approach, and Clinically-informed patch-level classification approach. Our CIMIL-CRC outperformed all methods (AUROC: 0.92 ± 0.002 (95% CI 0.91-0.92), vs. 0.79 ± 0.02 (95% CI 0.76-0.82), 0.86 ± 0.01 (95% CI 0.85-0.88), and 0.87 ± 0.01 (95% CI 0.86-0.88), respectively). The improvement was statistically significant. To the best of our knowledge, this is the best result achieved for MSI/MSS classification on this dataset. Our CIMIL-CRC method holds promise for offering insights into the key representations of histopathological images and suggests a straightforward implementation.

1. Introduction

The notable effectiveness of immunotherapy in treating solid tumors like melanoma and lung cancer has spurred interest in applying this method to colorectal cancer (CRC) Ganesh et al. (2019); Barzaman et al. (2021). However, the substantial variability both within and between CRC tumors complicates the success of immunotherapy Molinari et al. (2018); Li et al. (2020). Notably, immune-checkpoint inhibitors (ICIs) have demonstrated encouraging results in CRC patients with microsatellite instability (MSI), highlighting the crucial role of molecular subtyping in CRC for tailoring treatment plans Le et al. (2017); Hu et al. (2021).

Polymerase Chain Reaction (PCR) tests for DNA sequencing are currently the standard procedure for subtyping CRC Baudrin et al. (2018). However, these tests can be costly, time-intensive, and not universally accessible for all patients. In light of these challenges, convolutional neural networks (CNNs) He et al. (2016); Simonyan and Zisserman (2014) have been gaining traction as an automated alternative for identifying CRC subtypes. This method capitalizes on the widespread availabil-

ity of Hematoxylin and Eosin (H&E) stained histopathological images Kather et al. (2019); Kuntz et al. (2021); Wagner et al. (2023); Echle et al. (2020). The primary benefit of this approach is its use of images already produced in routine clinical settings, offering an efficient and precise means for CRC subtyping that can easily be integrated into existing clinical processes.

While the vast information content in H&E stained images is valuable for CRC subtyping, their extensive size, varying from 100 million to 10 billion pixels, poses a significant challenge to traditional graphics processing units (GPU) during model training, primarily due to memory limitations. To address the challenge of handling large H&E stained images, prior research has implemented a patch-based approach. This involves segmenting the images into smaller, more manageable sections for classification, followed by an aggregation of these results. For example, Kather et al. Kather et al. (2019) were at the forefront of using CNNs to determine CRC molecular subtypes (MSI and MSS) from H&E images. They utilized a patch-level classification technique and combined the outcomes using a majority vote, achieving a moderate level of success on the TCGA-CRC-DX database (with an area under the Receiver Operating Characteristic curve (AUROC) per patient of 0.77, $n=360$, 18% MSI). Following a similar methodology, Echle et al. Echle et al. (2020) enhanced overall classification accuracy by expanding

*Corresponding author: Moti Freiman, Tel.: +972-77-887-4147; Email: moti.freiman@technion.ac.il

the dataset size, and integrating multiple databases. However, their performance on the TCGA-CRC-DX cohort did not surpass that of Kather et al. Kather et al. (2019).

Yet, the classification of a WSI as either MSI or MSS pertains to the entire slide, not to individual patches. Consequently, only a fraction of the extracted patches may hold relevant information for this classification, with the remainder potentially being irrelevant. Therefore, a simplistic aggregation of patch-level classifications could potentially result in inaccuracies.

Multiple Instance Learning (MIL) frameworks are tailored for scenarios where each data sample is a ‘bag’ comprising numerous smaller subsamples, but labeled collectively as a single unit Carbonneau et al. (2018). In our context, each WSI is a ‘bag’, constituted by its individual patches, and is classified as either MSI or MSS. MIL methodologies have been effectively utilized in managing extensive WSI datasets across a range of medical applications Yao et al. (2020); Zhang et al. (2022); Shao et al. (2021); Sharma et al. (2021); Su et al. (2022); Qu et al. (2022).

In addressing the classification of CRC WSIs into MSI and MSS subtypes, Bilal et al. Bilal et al. (2021) applied an instance-level Multiple Instance Learning (MIL) strategy that focuses on identifying pivotal instances within a bag. Their ‘draw and rank’ technique iteratively progresses the top 5 patches from each patient through training. For the test set, WSI-level classification was based on the average scores of these patches, resulting in an average AUROC of 0.9 ± 0.01 and AUPRC of 0.72 ± 0.02 on the TCGA-CRC-DX database.

More recent efforts by Shats et al. Shats et al. (2022) involved a preprocessing stage to create lower-dimensional embeddings for each bag, subsequently undergoing bag-level classification and aggregation to derive WSI-level results. However, these bag-level approaches necessitate the selection of a fixed number of patches for each classification batch, which can be problematic as the number of patches with relevant information for classification may vary among different cases.

MIL classification techniques based on embedded representations offer an alternative by forgoing the necessity for fixed-size data. They operate in a condensed dimensional space that captures the essence of the entire WSI. For example, Hemati et al. utilized k-means clustering on RGB histograms from WSI patches to form a compressed WSI representation Hemati et al. (2021). They then selected random patch subsets from each cluster for WSI-level classification, using a consistent number of these embeddings. Fashi et al. enhanced this method by adding an attention mechanism to assign varying weights to different patches representing the WSI Fashi et al. (2022). Similarly, Sharma et al. developed an end-to-end system that creates embeddings for each patch and uses k-means clustering for WSI classification, selecting a fixed number of vectors from each cluster Sharma et al. (2021).

Despite these advancements, such approaches still necessitate selecting a certain number of patches or embeddings for final classification, risking information loss. Moreover, end-to-end training models require a substantial number of labeled WSIs, a challenging demand considering the typically small size of clinical WSI datasets Zhang et al. (2022).

Additionally, the scarcity of samples in these models limits their capability to generalize effectively across various tumor subtypes. Integrating specific clinical information could enhance their precision. For example, in CRC, tumors with the MSI classification are predominantly located in the ascending or proximal transverse colon (right-sided), while MSS tumors typically appear in the descending, sigmoid, and distal transverse colon (left-sided) Iacopetta (2002); Sugai et al. (2006). Notably, within the TCGA-CRC-DX cohort referenced in this study, 87% of MSI tumors are right-sided Kather et al. (2019).

In this work, we present ‘CIMIL-CRC,’ a Clinical-Informed Multiple Instance Learning (MIL) framework tailored for classifying CRC WSIs as either MSI or MSS. This model utilizes a refined, task-specific feature extractor to translate patch data into a latent space, followed by the consolidation of these patch embeddings through Principal Component Analysis (PCA). Classification at the WSI level is conducted by applying a classifier to the primary k principal components, representing the entire WSI. Our method stands out by incorporating all patches from a WSI via PCA on their embeddings, rather than selecting k key patches. We also improve the model’s adaptability to diverse tumor subtypes by integrating known clinical information regarding the tumor’s colonic location.

The ‘CIMIL-CRC’ model has achieved, to our best knowledge, unparalleled MSI/MSS classification accuracy on the TCGA-CRC-DX test-set cohort Kather et al. (2019).

The main contributions of our study are:

- Merging a pre-trained feature extraction model with Principal Component Analysis (PCA) for MIL-based WSI classification.
- Augmenting model accuracy through the inclusion of clinical prior knowledge.
- Surpassing existing benchmarks in MSI/MSS subtype classification of CRC using H&E stained WSI data from the TCGA-CRC-DX test-set cohort.

2. Related work

The standard DL-MIL algorithm for bag-level classification utilizes a variety of operators, including fully connected trainable layers and techniques like max-pooling, to derive the final WSI score. However, these operators have a noted limitation in trainability, as discussed in Ilse et al. (2018). To overcome this, an Attention mechanism was introduced, offering a trainable way to calculate a weighted sum of instances, thereby emphasizing crucial instances within the bag for WSI scoring. This mechanism also eliminates the need for bags to be of a fixed size.

Recent advancements have incorporated self-supervision into DL-MIL. Our study employed traditional supervision for feature extraction, but we will reference these developments for result comparison since they utilized the same TCGA-CRC-DX database ($n=360$) as our study.

DeepSMILE Schirris et al. (2022) applied the self-supervision method simCLR Chen et al. (2020a) for feature

extraction. This process involves augmenting each patch repeatedly and training the network to align the latent spaces of the same patch while differentiating those of distinct patches. An innovation in the Attention-based MIL field, VarMIL, calculates the variance within a bag’s latent spaces and combines it with the Attention MIL output before classification. The outcomes showed that simCLR alone (without MIL) achieved an AUROC of 0.87 ± 0.01 and an F1 score of 0.61 ± 0.11 . When combined with VarMIL, the results were an AUROC of 0.86 ± 0.02 and an F1 score of 0.47 ± 0.1 .

Another study Leiby et al. (2022) used supervised feature extraction with VGG19 (pre-trained on ImageNet), applying contrastive loss differently. Rather than comparing an augmented patch’s latent space to another augmented version, it was compared to its bag-level feature aggregation calculated via Attention. This method’s results indicated that Attention MIL alone yielded an AUROC of 0.86 ± 0.01 and an AUPRC of 0.73 ± 0.02 while adding contrastive loss improved the AUROC to 0.87 ± 0.01 and an AUPRC of 0.69 ± 0.04 .

In a different approach Saillard et al. (2021), self-supervision was used for feature extraction, combined with MIL models for patient aggregation. They employed Momentum Contrast v2 (MoCo v2Chen et al. (2020b)) for feature extraction on the CRC dataset and utilized the MIL models DeepMIL with attention Ilse et al. (2018) and Chowder Courtiol et al. (2018). The resulting AUROCs for these MIL models were 0.85(0.75-0.94) and 0.92(0.84-0.99) respectively.

3. Methods

We present a novel patient-level classification method, termed Clinically Informed Multiple Instance Learning for Colorectal Cancer (‘CIMIL-CRC’). The comprehensive architecture of this approach is depicted in Figure 1. The primary steps of our technique are as follows:

- **Feature Extraction (Figure 1 a):** In the initial phase, all patches are processed for feature extraction using a baseline model that has been pre-trained. The features derived from this stage encapsulate vital visual data, forming the basis for further analysis. These features are then systematically compiled into matrices specific to each patient.
- **Embedding Representation (Figure 1 b):** Using the patch-level features, we apply Principal Component Analysis (PCA) to construct a new patient-centric representation. This step effectively simplifies the feature space while maintaining key elements unique to each patient, thus optimizing computational efficiency without compromising on critical information.
- **Patient-level Classification (Figure 1 c-e):** Moving forward, the simplified feature representation facilitates patient-level classification via a Multi-Layer Perceptron (MLP). The integration of an Attention mechanism within our MLP enables it to synthesize insights from diverse patient components, leading to more comprehensive and precise patient-level assessments.

- **Clinical Data Incorporation (Figure 1 e):** We finally account for the significant difference in the anatomical location of MSI and MSS tumors in the colon by adjusting the classifier output by a predefined factor (Equation 4). This refinement boosts the efficacy of our model, culminating in the development of the CIMIL-CRC framework.

3.1. Feature extraction

We first implemented a baseline CNN model for patch-level binary classification (MSI/MSS) using a transfer-learning approach. To construct this model, we leveraged the pre-trained Efficient-net b7 architecture Tan and Le (2019), which had been originally trained on the extensive Imagenet database Deng et al. (2009). Fine-tuning was performed by retraining the last 7 blocks of layers, along with the fully connected layers, using our dataset. We saved a checkpoint of the trained baseline model.

Subsequently, we set the system in evaluation mode to derive features from every patch in both the training and test sets. These extracted features, with dimensions $[C, H, W] = [2560, 7, 7]$, offer a detailed and information-rich representation.

For enhanced higher-level examination, we arrange the gathered features for each patient into a matrix, which we denote as F_w . In the case of a patient with N patches, this matrix assumes the dimensions of $N \times d$, where d is calculated as $(7 \times 7 \times 2560)$. Every row in this matrix represents a flattened feature vector f_i derived from the i -th patch:

$$F_w = \begin{pmatrix} f_{11} & \cdots & f_{1d} \\ \vdots & \ddots & \vdots \\ f_{N1} & \cdots & f_{Nd} \end{pmatrix} \quad (1)$$

The number of patches varies from one patient to another, and accordingly, their feature matrices are saved. By structuring the features in this format, we efficiently consolidate and arrange the patch-level data into a format centered around each patient. This setup enables us to delve into patient-specific patterns and correlations, fostering deeper and more holistic analyses of the data.

3.2. Embedding representation

To facilitate patient-level classification, we sought a more condensed representation of our feature matrices. This approach enables us to process an entire patient’s data in a single instance and subsequently generate the network’s score for that patient.

To achieve this, we implemented the PCA method for a new, comprehensive data representation. This method also ensures the encapsulation of the entire original data set rather than selecting representative patches as suggested by previous MIL approaches.

For each patient, the extracted eigenvectors (EVs) delineate new axes in their feature space, effectively encapsulating the variance among features. To handle varying dimensionality, we chose the top-k EVs based on their eigenvalues, creating a new matrix for each patient $E_w \in \mathcal{R}^{k \times d}$.

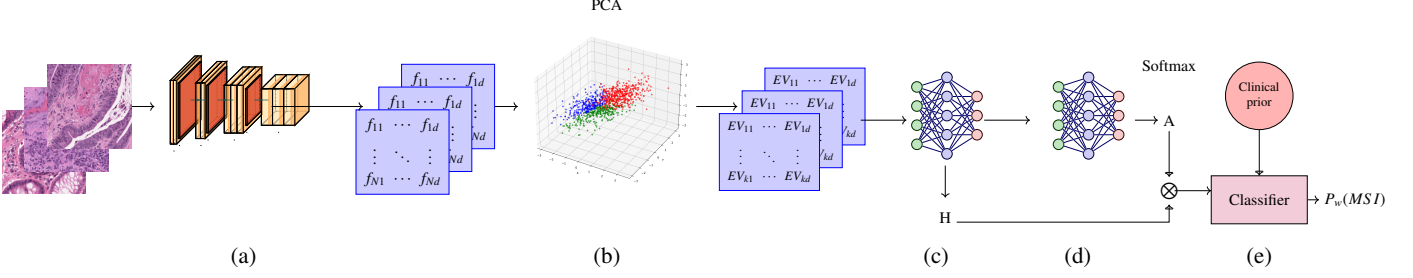


Figure 1: (a) Patches from each patient are processed through a pre-trained Efficient-net, operating in evaluation mode, to perform patch classification. This yields extracted features of dimension $[2560, 7, 7]$. These feature sets for each patient are then arranged into matrices and stored. (Image of CNN by Haris Iqbal Iqbal). (b) Principal Component Analysis (PCA) is subsequently applied to each patient’s feature matrix, retaining and saving the top- k eigenvectors (EVs). (c) These EV matrices are input into a Multi-Layer Perceptron (MLP) for further feature extraction, resulting in the matrix $H \in \mathcal{R}^{k \times 512}$. (d) Another MLP processes matrix H to create the Attention matrix $A \in \mathcal{R}^{k \times 3}$, followed by applying the Softmax function to its rows. (MLP illustration by Izaak Neutelings Neutelings (2021)). The matrices A and H are then combined through multiplication. (e) The combined output is flattened and introduced into a classifier MLP to determine the patient’s MSI score. This MSI score is subsequently adjusted by the side function (as described in Equation 4), generating the final patient-specific MSI score.

Nonetheless, considering that the maximum number of EVs that can be derived from the feature matrix is constrained by $\text{MIN}(n_{\text{samples}}, n_{\text{features}})$, there are instances where patients, particularly those with a smaller number of patches due to Kather et al.’s Kather et al. (2019) method of random patch sampling in MSS patients for patch-level data balancing in the training set, may yield fewer EVs. In such cases, we utilized the maximum possible number of EVs for these patients instead of excluding them from the analysis.

3.3. Patient-level classification

We then used the selected EVs as input to the DeepMIL with attention Glaser (2021); Ilse et al. (2018) classifier to obtain the patient-level classification as follows. The matrix of each patient’s K eigenvectors, E_w undergoes a feature extraction process through a Multi-Layer Perceptron (MLP), resulting in $H = F(E_w)$, $H \in \mathcal{R}^{K \times 512}$. The attention matrix is obtained as follows:

$$A = W_2(\tanh(W_1 \cdot H)) \odot W_3(\text{Sigmoid}(W_4 \cdot H)); A \in \mathcal{R}^{K \times 3} \quad (2)$$

Subsequently, we apply the Softmax function across the rows of A to normalize the weights. The final output probability for a patient’s MSI status is calculated using:

$$P_w(\text{MSI}) = \text{Sigmoid}(W_5(A^T \cdot H)) \quad (3)$$

3.3.1. Clinical Data Incorporation

Finally, we incorporated the clinical prior associated with the anatomical side of the tumor by adjusting the classifier’s output according to the Bayes rule. As indicated by prior research Iacopetta (2002); Sugai et al. (2006) and consistent with the data trends in the TCGA-CRC-DX cohort referenced in this study Kather et al. (2019), about 90% of MSI tumors are found on the right side. We therefore defined the side prior function based on the tumor’s location as:

$$\text{Prior} = f(\text{side}) = \begin{cases} 0.1 & \text{side} = \text{Left} \\ 0.9 & \text{side} = \text{Right/undefined} \end{cases} \quad (4)$$

Training settings. We used the binary cross entropy (BCE) loss with label smoothing Christian et al. (2015) as our loss function to tackle the over-fitting and over-confidence of the classifier. We accounted for data imbalance in the training dataset by incorporating class-related weights into the loss function. We calculated the class weights as the inverse proportion of each patient’s class representation.

We employed the ADAM optimizer for training with the following parameters: betas set to (0.7, 0.99), an initial learning rate of 0.0001, a training duration of 10 epochs, and a batch size configured for one patient. Model checkpoints were saved whenever MSI accuracy and overall accuracy exceeded 95%. The cross-validation folds were stratified, aligning with the baseline methodology. We implemented our code using PyTorch 1.9 and ran it on Nvidia A100 GPUs using a PyTorch NGC Container, version 21.04.

4. Experiments

4.1. Dataset

Our research utilized the TCGA-CRC-DX cohort from The Cancer Genome Atlas (TCGA) Kather (2019), which comprises data from $n=360$ patients. This cohort consists of formalin-fixed paraffin-embedded (FFPE) diagnostic slides that are H&E stained from colorectal cancer (CRC) patients. Additionally, the database provides results of DNA mutations, RNA expression, and clinical annotations. MSI/MSS reference labels were determined by Liu et al. (2018) (as referenced in Supplementary Table 2 of Kather et al. (2019)). Kather et al. pre-processed and published this data, with the steps detailed in Kather et al. (2019).

Figure 2 illustrates the distribution of patients in the dataset. During the pre-processing phase, a random selection of 100 out of the 360 patients was set aside as a test set Kather et al. (2019). In the training set, 15% of patients are classified as MSI, while the test set contains 26% MSI patients. Multiple image patches were extracted from each H&E slide, and the training set was balanced at the patch level by selectively discarding MSS patches.

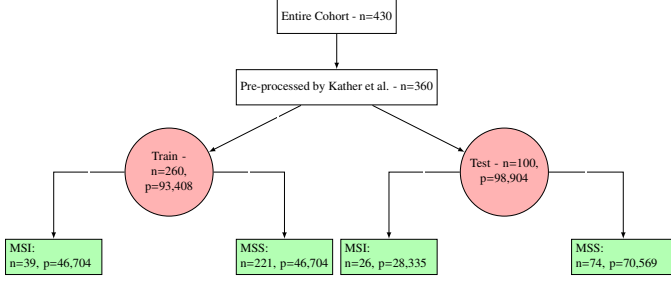


Figure 2: Data preprocessing chart. From the TCGA-CRC cohort (n=430), Kather et al. selected and pre-processed a subset (n=360) for publication. This subset was divided into a training set (n=260) and a testing set (n=100). Balancing was applied at the patch level within the training set by excluding MSS patches.

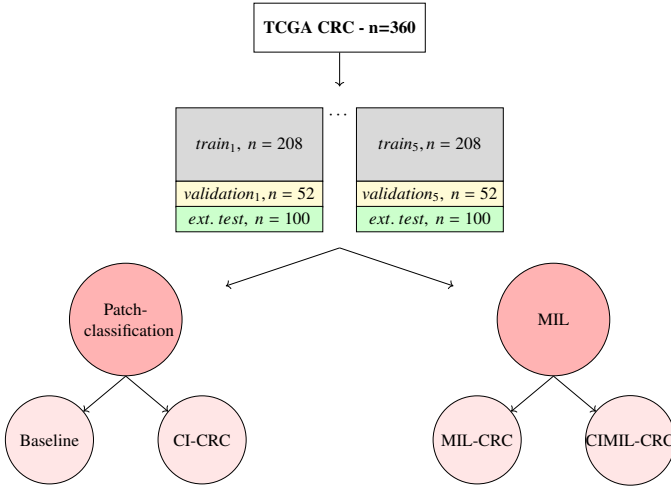


Figure 3: Our external test set consists of n=100 patients, randomly selected by Kather et al. from their total cohort of n=360 Kather et al. (2019). The remaining n=260 patients were meticulously divided into 5 stratified folds to enable cross-validation, ensuring a balanced class distribution across these folds. We evaluated the efficacy of our methods using the AUC, F1, and Cohen’s-Kappa scores, applied to each fold’s model on the external test set. This evaluation was conducted for both the patch classification models and our MIL-based models (MIL-CRC, CIMIL-CRC). Additionally, for a comprehensive comparison, we incorporated the clinical information prior also to the patch-classification model (resulting in CI-CRC).

4.2. Experimental methodology

Fig. 3 provides an overview of our experimental approach. Initially, we detail the various models deployed in our assessment, followed by a description of our evaluation methodology.

4.2.1. Classification models

We evaluated the distinct contribution of each component in our CIMIL-CRC methodology, by conducting comparative analyses with various models in addition to our CIMIL-CRC model as follows:

- **Baseline Model:** This model served as our point of reference. It primarily focused on patch-level classification with patient aggregation conducted externally to the CNN.

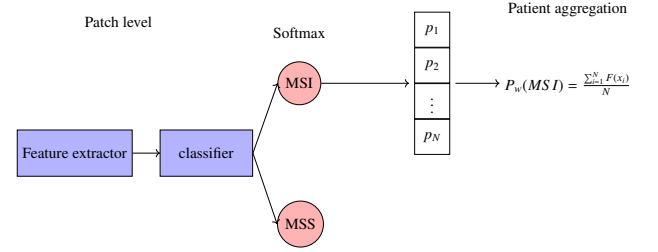


Figure 4: Baseline Model Architecture. Patches are fed into the Efficient-net b7 for feature extraction. The last two layers consist of fully connected classifier layers. The outputs then pass through a Softmax layer to generate probabilities. N represents the number of patches for each patient, with $F(x_i)$ denoting the MSI probabilities of these patches. The MSI score for each patient, P_w , is calculated as the average of these MSI probabilities.

- **CI-CRC - Clinical Information Enhanced Baseline Model:** This version enhances the baseline model by incorporating clinical side information during patient aggregation, allowing us to assess its contribution to overall model performance in comparison to other approaches.
- **MIL-CRC** Our main model utilizes our PCA-based MIL approach (MIL-CRC) but without adjusting the model output with the side prior function.

Baseline model

Figure 4 illustrates the baseline model architecture employed in our research. It utilizes an Efficient-net b7 as the CNN to classify patches into MSI/MSS categories. Patch-level classifications are combined into a patient-level classification by averaging the probabilities of patch classification. Specifically, for a classifier F , the output for a given patch x represents the probability that it belongs to the MSI class, with $(0 \leq F(x) \leq 1)$.

For an H&E slide W , N patches (x_1, x_2, \dots, x_N) are extracted from W . The MSI probability at the patient level is then calculated as follows:

$$P_w(\text{MSI}) = \frac{\sum_{i=1}^N F(x_i)}{N} \quad (5)$$

CI-CRC - Baseline model with clinical side Information

A baseline patch-level classification model employing a consolidated score for patient-level classification, as defined in Eq. 5, complemented by the integration of clinical side information. This integration involves multiplying the patient score (Eq. 5) with the side prior function (Eq. 4).

MIL-CRC model

Our main PCA-based MIL model, without integrating clinical side information as a prior.

4.2.2. Evaluation methodology

We started with hyperparameters optimization. Specifically, we consider the optimal number of EVs necessary for accurately representing a patient and the impact of different label smoothing rates on the classification performance. We determined the optimal number of EVs to use by utilizing

the CIMIL-CRC model with an EV input range of [1, 120]. For each specified number of EVs, we conducted a stratified 5-fold cross-validation, followed by an analysis of the average F1-score and Cohen’s-kappa results on the validation set across the folds, considering the number of EVs as input to the final classifier. Additionally, we tested smoothing rates of [0, 0.01, 0.02, 0.03].

Subsequently, we trained the various models (Baseline, CI-CRC, MIL-CRC, CIMIL-CRC) using a stratified 5-fold cross-validation method, resulting in five trained models for each approach.

In the final phase, we compared the MSI/MSS classification accuracy of these models on the test-set provided by Kather et al. Kather et al. (2019). We used the area under the ROC curve (AUROC), the area under the precision-recall curve (AUPRC), the average precision (AP), the F1- score, and the Cohen’s-kappa score as our evaluation metrics. A paired Student’s t-test with a significance level of $p < 0.05$ was employed to ascertain the statistical significance of the improvements observed with MIL-CRC and CIMIL-CRC compared to the Baseline models.

5. Results

Fig. 5 illustrates the average accuracy of our CIMIL-CRC model across the 5 validation set folds, plotted against the number of EVs inputted into the final patient-level classifier.

Through our analysis, it was determined that using 90 EVs produced the highest average F1-score and Cohen’s-kappa score across the validation sets. Furthermore, we identified that label smoothing rates of $\alpha = 0.01$ or $\alpha = 0.03$ resulted in the most favorable average F1-score and Cohen’s-kappa score. These hyper-parameters were employed to train the models across various folds for our experimental analysis on the test set provided by Kather et al. Kather et al. (2019).

Table 1 presents a comparative analysis of our various models. The MIL-CRC model demonstrated a significantly higher average AUROC (0.86 ± 0.01 , 95% CI 0.85-0.88, compared to 0.79 ± 0.02 , 95% CI 0.76-0.82, with a paired t-test p -value < 0.01) and Average Precision (AP) (0.8 ± 0.02 , 95% CI 0.77-0.82, versus 0.64 ± 0.04 , 95% CI 0.58-0.68, with a paired t-test p -value < 0.01) compared to the baseline patch-level model. Similarly, the CIMIL-CRC, which integrates clinical side information into our MIL framework, showed improved classification accuracy compared to the CI-CRC, which is the clinical information integrated baseline patch-level model. This improvement is evidenced in both AUROC (0.92 ± 0.002 , 95% CI 0.91-0.92, versus 0.88 ± 0.007 , 95% CI 0.87-0.88, with a paired t-test p -value < 0.001) and AP (0.86 ± 0.01 , 95% CI 0.84-0.87, compared to 0.81 ± 0.01 , 95% CI 0.79-0.81, with a paired t-test p -value < 0.01).

Fig. 6 displays the ROC curves and the Precision-Recall curves for these different models on the test set provided by Kather et al. Kather et al. (2019).

Table 2 showcases the performance of our CIMIL-CRC approach relative to recent state-of-the-art methods applied to the dataset from Kather et al. Kather et al. (2019). Our method surpasses most others, particularly in terms of AUPRC, by a

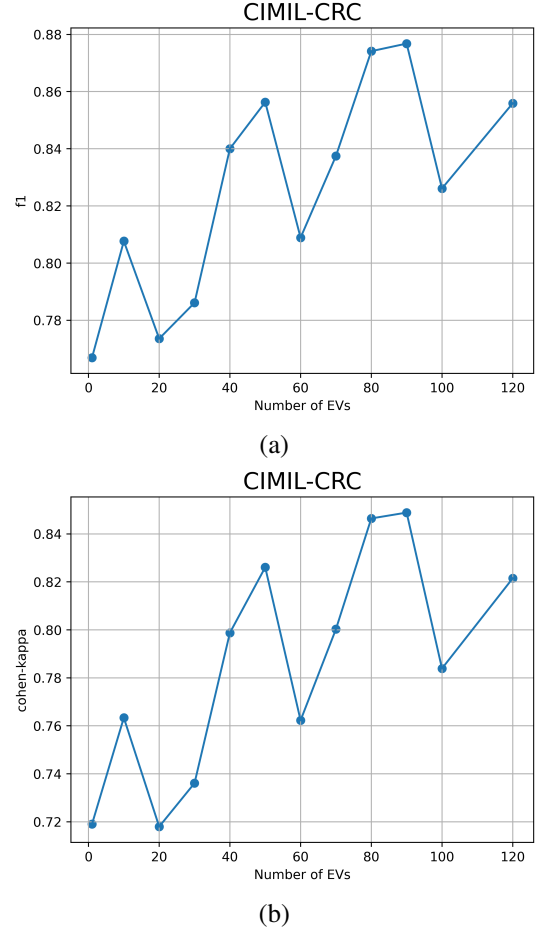


Figure 5: Results of the validation sets, averaged over the 5-folds for varying number of EVs. (a) F1-score, (b) Cohen’s-kappa score.

significant margin. It achieves an AUROC comparable to that of Saillard et al. Saillard et al. (2021) but with a notably smaller standard deviation. It’s crucial to highlight that while Saillard et al. utilized additional data beyond the TCGA-CRC-DX dataset for training, our approach did not. Furthermore, we provide AUPRC and F1-score metrics, which are not reported by Saillard et al., making a direct comparison somewhat complex.

6. Conclusions

We introduce CIMIL-CRC, a clinically-informed multiple-instance learning (MIL) strategy for categorizing Hematoxylin and Eosin (H&E) stained whole-slide images (WSI) of colorectal cancer (CRC) into microsatellite instability (MSI) and microsatellite stable (MSS) subtypes. Contrary to previous MIL patient-level classification methods, which prioritized selecting representative patches and discarding less informative ones Schirris et al. (2022); Bilal et al. (2021), our approach generates a patient-level embedding space by applying PCA decomposition to patch-level features. Additionally, we incorporate clinical information, specifically tumor location, to improve classification accuracy. Our experiments, conducted in 5 folds on the TCGA-CRC-DX dataset Kather (2019); Kather et al. (2019), have shown our approach’s superiority over existing methods

Method	AUROC(95% CI)	AUPRC(95% CI)	F1	C-K
Baseline	0.79(0.76-0.79)	0.64(0.58-0.68)	0.63(0.58-0.66)	0.52(0.44-0.58)
CI-CRC	0.88(0.87-0.88)	0.8(0.79-0.81)	0.72(0.69-0.76)	0.63(0.56-0.68)
MIL-CRC	0.86(0.85-0.88)	0.8(0.77-0.82)	0.75(0.73-0.78)	0.67(0.64-0.71)
CIMIL-CRC	0.92(0.91-0.92)	0.86(0.84-0.87)	0.8(0.79-0.82)	0.73(0.72-0.76)

Table 1: Performance of our MIL-CRC methods (MIL-CRC and CIMIL-CRC), averaged over 5 folds with 95% confidence intervals, compared to the patch-classification methods (baseline and CI-CRC).

Method	AUROC(\pm std)	AUPRC(\pm std)	F1
Bilal et al. (2021)	0.9 \pm 0.01	0.72 \pm 0.02	-
simCLR+VarMIL Schirris et al. (2022)	0.86 \pm 0.02	-	0.47 \pm 0.1
simCLR+patch classification Schirris et al. (2022)	0.87 \pm 0.01	-	0.61 \pm 0.11
MIL Leiby et al. (2022)	0.86 \pm 0.01	0.73 \pm 0.02	-
MIL+contrastive Leiby et al. (2022)	0.87 \pm 0.01	0.69 \pm 0.04	-
Moco+MIL Saillard et al. (2021)	0.92(0.84-0.99)	-	-
MIL-CRC(ours)	0.86 \pm 0.01	0.8 \pm 0.02	0.75 \pm 0.02
CIMIL-CRC(ours)	0.92\pm0.002	0.86\pm0.01	0.8\pm0.01

Table 2: Performance of our MIL methods (MIL-CRC and CIMIL-CRC), averaged over 5 folds with 95% confidence intervals, compared to reported published results (validated by their protocol).

on the same dataset. Moreover, we have identified the distinct contributions of each aspect of our method, including the PCA-based MIL and the integration of clinical information.

Our proposed methodology not only emphasizes the critical role of patient-level aggregation in MIL-based classification but also highlights the significance of integrating prior knowledge and its effect on model performance. This approach shows promise for further application in other MIL-based tasks using H&E WSI data.

Acknowledgements

M.F. acknowledges funding from the Israel Innovation Authority (grant number 73249) and from Microsoft Education and the Israel Inter-university computation center (IUCC). Y.E.M. acknowledges funding from the Israel science foundation (ISF, grant number 2794/21) and from the Israel cancer association (ICA, grant number 20210132).

Declaration of Generative AI

During the preparation of this work, the author(s) used ChatGPT in order to improve readability. After using this tool/service, the author(s) reviewed and edited the content as needed and take(s) full responsibility for the content of the publication.

References

Barzaman, K., Moradi-Kalbolandi, S., Hosseinzadeh, A., Kazemi, M.H., Khorramdelazad, H., Safari, E., Farahmand, L., 2021. Breast cancer immunotherapy: Current and novel approaches. *Int. Immunopharmacol.* 98, 107886.

Baudrin, L.G., Deleuze, J.F., How-Kit, A., 2018. Molecular and computational methods for the detection of microsatellite instability in cancer. *Front. Oncol.* 8, 621.

Bilal, M., Raza, S.E.A., Azam, A., Graham, S., Ilyas, M., Cree, I.A., Snead, D., Minhas, F., Rajpoot, N.M., 2021. Development and validation of a weakly supervised deep learning framework to predict the status of molecular pathways and key mutations in colorectal cancer from routine histology images: a retrospective study. *The Lancet Digital Health* doi:10.1016/s2589-7500(21)00180-1.

Carbonneau, M.A., Cheplygina, V., Granger, E., Gagnon, G., 2018. Multiple instance learning: A survey of problem characteristics and applications. *Pattern Recognition* 77, 329–353.

Chen, T., Kornblith, S., Norouzi, M., Hinton, G., 2020a. A simple framework for contrastive learning of visual representations, in: *International conference on machine learning*, PMLR. pp. 1597–1607.

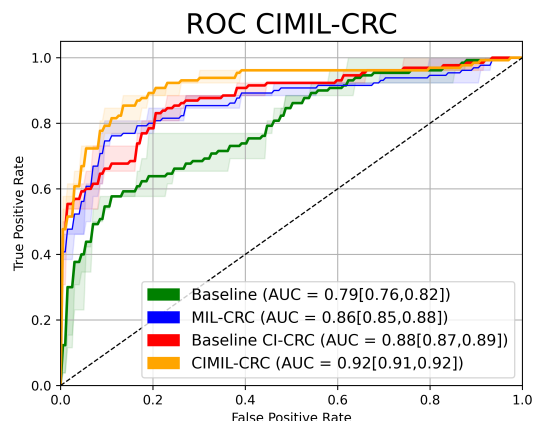
Chen, X., Fan, H., Girshick, R., He, K., 2020b. Improved baselines with momentum contrastive learning. *arXiv preprint arXiv:2003.04297*.

Christian, S., Vincent, V., Sergey, I., Jonathon, S., Zbigniew, W., 2015. Rethinking the inception architecture for computer vision. *CoRR abs/1512.00567*. URL: <http://arxiv.org/abs/1512.00567>, arXiv:1512.00567.

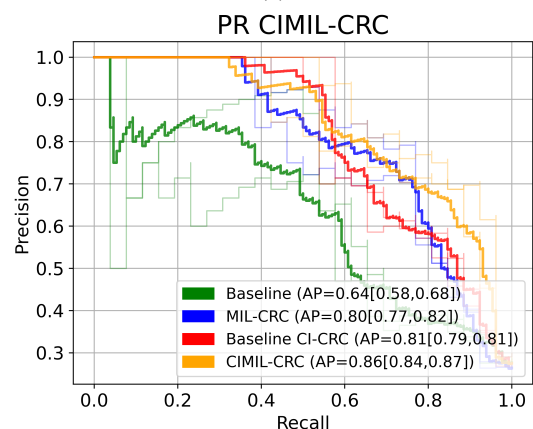
Courtillot, P., Tramel, E.W., Sanselme, M., Wainrib, G., 2018. Classification and disease localization in histopathology using only global labels: A weakly-supervised approach. *arXiv preprint arXiv:1802.02212*.

Deng, J., Dong, W., Socher, R., Li, L.J., Li, K., Fei-Fei, L., 2009. Imagenet: A large-scale hierarchical image database, in: *2009 IEEE conference on computer vision and pattern recognition*, Ieee. pp. 248–255.

Echle, A., Grabsch, H., Quirke, P.e.a., 2020. Clinical-Grade Detection of Microsatellite Instability in Colorectal Tumors



(a)



(b)

Figure 6: Plots of MIL-CRC and CIMIL-CRC conducted with 90 EVs plotted vs. the baseline patch classification and baseline with clinical side integration. (a) ROC (b) PR.

by Deep Learning. *Gastroenterology* 159, 1406–1416. doi:doi:10.1053/j.gastro.2020.06.021.

Fashi, P.A., Hemati, S., Babaie, M., Gonzalez, R., Tizhoosh, H., 2022. A self-supervised contrastive learning approach for whole slide image representation in digital pathology. *Journal of Pathology Informatics* 13, 100133. URL: <https://www.sciencedirect.com/science/article/pii/S2153353922007271>, doi:<https://doi.org/10.1016/j.jpi.2022.100133>.

Ganesh, K., Stadler, Z.K., Cercek, A., Mendelsohn, R.B., Shia, J., Segal, N.H., Diaz, Jr, L.A., 2019. Immunotherapy in colorectal cancer: rationale, challenges and potential. *Nat. Rev. Gastroenterol. Hepatol.* 16, 361–375.

Glaser, J., 2021. Attention Based Deep Multiple Instance Learning. <https://github.com/jmg764/Attention-Based-Deep-Multiple-Instance-Learning>.

He, K., Zhang, X., Ren, S., Sun, J., 2016. Deep residual learning for image recognition, in: *Proceedings of the IEEE conference on computer vision and pattern recognition*, pp. 770–778.

Hemati, S., Kalra, S., Meaney, C., Babaie, M., Tizhoosh, H.R., 2021. CNN and Deep Sets for End-to-End Whole Slide Image Representation Learning. *Proceedings of Machine Learning Research* 143.

Hu, L.F., Lan, H.R., Huang, D., Li, X.M., Jin, K.T., 2021. Personalized Immunotherapy in Colorectal Cancers: Where Do We Stand? doi:10.3389/fonc.2021.769305.

Iacopetta, B., 2002. Are there two sides to colorectal cancer? *Int. J. Cancer* 101, 403–408.

Ilse, M., Tomczak, J.M., Welling, M., 2018. Attention-based deep multiple instance learning.

Iqbal, H., . Plotneuralnet. <https://zenodo.org/record/2526396>.

Kather, J.N., 2019. Histological images for MSI vs. MSS classification in gastrointestinal cancer, FFPE samples. URL: <https://doi.org/10.5281/zenodo.2530835>, doi:10.5281/zenodo.2530835.

Kather, J.N., Pearson, A.T., Halama, N.e.a., 2019. Deep learning can predict microsatellite instability directly from histology in gastrointestinal cancer. *Nature Medicine* 25, 1054–1056. URL: <http://www.nature.com/articles/s41591-019-0462-y>, doi:10.1038/s41591-019-0462-y.

Kuntz, S., Kriehoff-Henning, E., Kather, J.N., Jutzi, T., Höhn, J., Kiehl, L., Hekler, A., Alwers, E., von Kalle, C., Fröhling, S., et al., 2021. Gastrointestinal cancer classification and prognostication from histology using deep learning: Systematic review. *European Journal of Cancer* 155, 200–215.

Le, D.T., Durham, J.N., Smith, K.N., Wang, H., Bartlett, B.R., Aulakh, L.K., Lu, S., Kemberling, H., Wilt, C., Luber, B.S., et al., 2017. Mismatch repair deficiency predicts response of solid tumors to pd-1 blockade. *Science* 357, 409–413.

Leiby, J.S., Hao, J., Kang, G.H., Park, J.W., Kim, D., 2022. Attention-based multiple instance learning with self-supervision to predict microsatellite instability in colorectal cancer from histology whole-slide images, in: *2022 44th Annual International Conference of the IEEE Engineering in Medicine & Biology Society (EMBC)*, IEEE. pp. 3068–3071.

Li, K., Luo, H., Huang, L., Luo, H., Zhu, X., 2020. Microsatellite instability: a review of what the oncologist should know. *Cancer Cell Int.* 20, 16.

Liu, Y., Sethi, N.S., Hinoue, T., Schneider, B.G., Cherniack, A.D., Sanchez-Vega, F., Seoane, J.A., Farshidfar, F., Bowlby, R., Islam, M., Kim, J., Chatila, W., Akbani, R., Kanchi, R.S., Rabkin, C.S., Willis, J.E., Wang, K.K., McCall, S.J., Mishra, L., Ojesina, A.I., Bullman, S., Pedamallu, C.S., Lazar, A.J., Sakai, R., 2018. Comparative Molecular Analysis of Gastrointestinal Adenocarcinomas. *Cancer Cell* 33, 721–735. doi:10.1016/J.CCELL.2018.03.010.

- Molinari, C., Marisi, G., Passardi, A., Matteucci, L., De Maio, G., Ulivi, P., 2018. Heterogeneity in colorectal cancer: a challenge for personalized medicine? *International journal of molecular sciences* 19, 3733.
- Neutelings, I., 2021. Neural networks. https://tikz.net/neural_networks/.
- Qu, L., Luo, X., Liu, S., Wang, M., Song, Z., 2022. Dgmil: Distribution guided multiple instance learning for whole slide image classification, in: *International Conference on Medical Image Computing and Computer-Assisted Intervention*, Springer. pp. 24–34.
- Saillard, C., Dehaene, O., Marchand, T., Moindrot, O., Kamoun, A., Schmauch, B., Jegou, S., 2021. Self supervised learning improves dmmr/msi detection from histology slides across multiple cancers. *arXiv preprint arXiv:2109.05819*.
- Schirris, Y., Gavves, E., Nederlof, I., Horlings, H.M., Teuwen, J., 2022. Deepsmile: contrastive self-supervised pre-training benefits msi and hrd classification directly from h&e whole-slide images in colorectal and breast cancer. *Medical Image Analysis* 79, 102464.
- Shao, Z., Bian, H., Chen, Y., Wang, Y., Zhang, J., Ji, X., et al., 2021. Transmil: Transformer based correlated multiple instance learning for whole slide image classification. *Advances in neural information processing systems* 34, 2136–2147.
- Sharma, Y., Shrivastava, A., Ehsan, L., Moskaluk, C.A., Syed, S., Brown, D., 2021. Cluster-to-conquer: A framework for end-to-end multi-instance learning for whole slide image classification, in: *Medical Imaging with Deep Learning*, PMLR. pp. 682–698.
- Shats, D., Hezi, H., Shani, G., Maruvka, Y.E., Freiman, M., 2022. Patient-level microsatellite stability assessment from whole slide images by combining momentum contrast learning and group patch embeddings, in: *European Conference on Computer Vision*, Springer. pp. 454–465.
- Simonyan, K., Zisserman, A., 2014. Very deep convolutional networks for large-scale image recognition. *arXiv preprint arXiv:1409.1556*.
- Su, Z., Tavolara, T.E., Carreno-Galeano, G., Lee, S.J., Gurcan, M.N., Niazi, M., 2022. Attention2majority: Weak multiple instance learning for regenerative kidney grading on whole slide images. *Medical Image Analysis* 79, 102462.
- Sugai, T., Habano, W., Jiao, Y.F., Tsukahara, M., Takeda, Y., Otsuka, K., Nakamura, S.i., 2006. Analysis of molecular alterations in left-and right-sided colorectal carcinomas reveals distinct pathways of carcinogenesis: proposal for new molecular profile of colorectal carcinomas. *The Journal of Molecular Diagnostics* 8, 193–201.
- Tan, M., Le, Q.V., 2019. EfficientNet: Rethinking model scaling for convolutional neural networks.
- Wagner, S.J., Reisenbüchler, D., West, N.P., Niehues, J.M., Veldhuizen, G.P., Quirke, P., Grabsch, H.I., Brandt, P.A., Hutchins, G.G., Richman, S.D., et al., 2023. Fully transformer-based biomarker prediction from colorectal cancer histology: a large-scale multicentric study. *arXiv preprint arXiv:2301.09617*.
- Yao, J., Zhu, X., Jonnagaddala, J., Hawkins, N., Huang, J., 2020. Whole slide images based cancer survival prediction using attention guided deep multiple instance learning networks. *Medical Image Analysis* 65, 101789.
- Zhang, H., Meng, Y., Zhao, Y., Qiao, Y., Yang, X., Coupland, S.E., Zheng, Y., 2022. Dtf-d-mil: Double-tier feature distillation multiple instance learning for histopathology whole slide image classification, in: *Proceedings of the IEEE/CVF Conference on Computer Vision and Pattern Recognition*, pp. 18802–18812.